ChemComm

COMMUNICATION

View Article Online
View Journal | View Issue

Check for updates

Cite this: *Chem. Commun.*, 2023, 59, 14126

Received 31st August 2023,
Accepted 27th October 2023

DOI: 10.1039/d3cc04308h

rsc.li/chemcomm

Published on 27 Diteli 2023. Downloaded on 19/07/2025 10:58:16 AM.

Two-dimensional lead-free silver-bismuth double perovskite nanobelts with intrinsic chirality *via* co-antisolvent modulation strategy†

Xuexia Yu,[a] Rong Lu,[a] Pengfei Zhang,[a] Shun Wang,[ab] Yihuang Chen *[ab] and Shuang Pan *[ab]

This study presents an optimized co-antisolvent modulation strategy for producing two-dimensional lead-free chiral double perovskite nanomaterial with superior chirality and stability. The chiroptical signals or their dissymmetric factors are significantly influenced by the selection of antisolvent mixture. This research contributes to the advancement of chiral semiconductor materials and expands the understanding of their behavior at the nanoscale.

Chiral 2D organic–inorganic hybrid perovskites (OIHPs) represent an intriguing class of materials that combine the excellent crystallinity and exciton properties inherent in 2D perovskites, as well as the unique chiral optoelectronic and spintronic properties derived from its chirality.[1,2] The incorporation of chiral OIHPs into various optoelectronic systems presents exciting opportunities for advanced technologies in circularly polarized luminescence (CPL) detection spin modulation, nonlinear optics, bulk photovoltaics, ferroelectrics, and more.[3,4] However, the majority of reported chiral perovskites contain high concentrations of toxic lead ions and exhibit stability issues, which significantly impede their feasibility for large-scale production and practical use.[5] The substitution of lead with tin (Sn) is an attractive choice based on valence state considerations. However, the susceptibility of Sn^{II} to oxidation, resulting in the formation of Sn^{IV} and potential material defects within the material, poses a significant challenge to lead-free tin-based low-dimensional chiral perovskite.[6] Therefore, it is imperative to prioritize the development of stable low-dimensional lead-free chiral perovskites and conduct comprehensive investigations into their structure–property relationships.

As an alternative, emerging 2D analogues of chiral double perovskites, incorporating trivalent cations (*e.g.*, Bi^{3+}) and monovalent cations (*e.g.*, Ag^{+}), are being explored as next-generation candidates due to their distinct advantages of non-toxicity, phase stability, and intriguing chiroptical properties. Recent advancements in synthesizing macroscopic single crystals based on chiral silver-bismuth (Ag–Bi) double perovskites had demonstrated immense potential in the field of circularly polarized light-sensitive detection and self-powered X-ray detection.[7,8] Inevitably, the challenges associated with the utilization of corrosive acid solutions and the resulting pollution, as well as the stringent requirements for temperature control and time-consuming processes in single crystal growth, pose significant obstacles to large-scale production.[1] Additionally, the resultant single crystals often exceed the nanoscale in size, lacking desirable colloidal dispersity and solution processability, limiting the detailed investigation of size and structure-dependent characteristics of chiral perovskite nanomaterials.[9] Fortunately, colloidal 2D halide perovskites can be conveniently prepared by an organic antisolvent to impart supersaturated precipitation caused by solubility changes, eliminating the requirement for heating and hydrohalic acids.[10] Despite the impressive enlightenment, the implementation of antisolvent modulation for chiral double perovskite nanomaterials, especially Ag–Bi-based systems, has rarely been reported. Moreover, it is important to highlight that various factors, including the structure of chiral organic spacer cations, the selection of polarity solvents or anti-solvents, and the choice of ligands can exert significant influence on the morphology, symmetry and the growth of chiral perovskite nanocrystals.[9] The interplay between these factors determines whether the resulting crystals are bulk-sized or confined to the nanoscale, as well as influencing the final shape and dimensionality chiroptical properties of the chiral halide perovskites nanomaterials. This, however, has yet to be explored in the chiral double perovskite nanomaterials.

In this work, we present a convenient synthesis route to chiral Ag–Bi double perovskite nanomaterials with compelling chirality and stability. The key to our strategy lies in the precise

[a] *College of Chemistry and Materials Engineering, Wenzhou University, Wenzhou 325035, China. E-mail: yhchen@wzu.edu.cn, shuangpan@wzu.edu.cn*
[b] *Institute of New Materials and Industrial Technologies, Wenzhou University, Wenzhou 325035, China*

† Electronic supplementary information (ESI) available. See DOI: https://doi.org/10.1039/d3cc04308h

This journal is © The Royal Society of Chemistry 2023

Published on 27 Diteli 2023. Downloaded on 19/07/2025 10:58:16 AM.

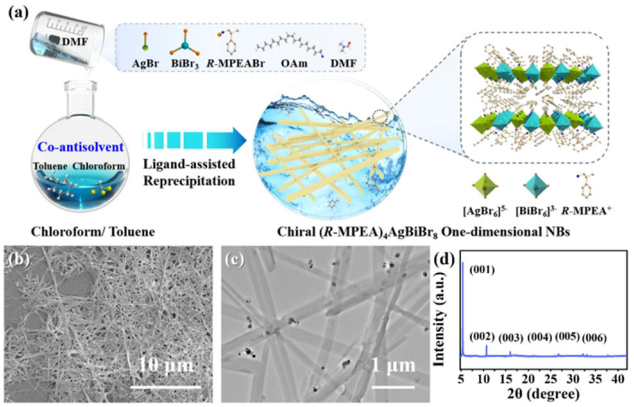

Fig. 1 (a) Schematic illustration of co-antisolvent modulation strategy *via* LARP for the synthesis, (b) SEM, (c) TEM images and (d) XRD pattern of the 2D double perovskite $(R\text{-MPEA})_4AgBiBr_8$ NBs.

modulation of antisolvent composition during the ligand-assisted reprecipitation (LARP) method. The co-antisolvent plays a crucial role in controlling the morphology of the resulting 2D chiral Ag–Bi double perovskite nanomaterials. Concretely, the formation of one-dimensional shape chiral Ag–Bi double perovskite nanobelts (NBs) is driven quickly once the precursor solution was injected into the co-antisolvent mentioned above. These NBs exhibit the largest g_{abs}-factor (at 420 nm) of -1.43×10^{-3}, indicating that the optical transitions originating from the inorganic sublattice acquire a chiral response. Additionally, these chiral Ag–Bi double perovskite NBs displayed tuneable photoluminescence and superior stability. Our study opens up new possibilities for conducting fundamental studies and exploring the chiroptical applications of these intriguing materials.

Fig. 1a schematically depicted the facile co-antisolvent modulation strategy of LARP method for the preparation of the chiral 2D lead-free double perovskite nanomaterial at room temperature (see Experimental Section for detail, ESI†). It is worth noting that employing an appropriate antisolvent and controlling its content are the key steps in these process to obtain desired nanocrystal properties successfully, ensuring control over thickness, morphology, and its optical behaviour. Here, a mixture of chloroform/toluene solution in the volume ratio of 2 : 3 served as the co-antisolvent and the precise manipulation in antisolvent to achieve the satisfied properties of the 2D double perovskite $(R\text{-MPEA})_4AgBiBr_8$ NBs is presented.

The structure and morphological characteristics of 2D double perovskite $(R\text{-MPEA})_4AgBiBr_8$ NBs were first scrutinized. The scanning electron microscope (SEM) image was displayed in Fig. 1b, revealing the presence of one-dimensional NBs of double perovskite $(R\text{-MPEA})_4AgBiBr_8$. The large-scale SEM image is presented in Fig. S1 (ESI†), revealing that these nanobelts are not limited to localized formation. The width of the NBs was 150 ± 40 nm, while the height of the NBs was 30 ± 5 nm as determined by the representative TEM (Fig. 1c) and AFM measurements (Fig. S2, ESI†). The corresponding histograms (Fig. S3, ESI†) demonstrated a uniform distribution of widths and heights among the $(R\text{-MPEA})_4AgBiBr_8$ NBs. The X-ray diffraction (XRD) pattern of the 2D $(R\text{-MPEA})_4AgBiBr_8$ NBs exhibited distinct Bragg diffraction peaks at angles of 5.5°, 11°, and 18°, corresponding to the (00*l*) crystal planes of the 2D double perovskite structure, which provides evidence of their crystalline nature and closely resembles that of the chiral iodine analogues $(R\text{-MPEA})_4AgBiI_8$ single crystal (Fig. 1d).[10] The absence of any impurity peaks in the obtained spectra suggests the phase purity of the $(R\text{-MPEA})_4AgBiBr_8$ NBs. The calculated out-of-plane distance of 2 nm was similar to that of $(PEA)_4AgBiBr_8$ perovskite microplates,[11] suggesting that the $(R\text{-MPEA})_4AgBiBr_8$ NBs also consisted of a single atomic layer of inorganic octahedron. These results together with the energy dispersive X-ray spectroscopy (EDS; Fig. S4, ESI†) and X-ray photoelectron spectroscopy (XPS; Fig. S5, ESI†) substantiated the successful synthesis of $(R\text{-MPEA})_4AgBiBr_8$ NBs. The dark spots with higher contrast observed in NBs can be ascribed to the formation of metallic silver clusters (Fig. S6, ESI†).

The optical properties of the synthesized 2D $(R\text{-MPEA})_4AgBiBr_8$ NBs were investigated to gain insight into their chiroptical behaviour (Fig. 2 and Fig. S7, ESI†). The UV absorption peak was observed at around 405 nm, while the photoluminescence (PL) emission peak was located in the blue region at approximately 470 nm (Fig. 2a). Temperature-dependent PL spectra analysis was performed on $(R\text{-MPEA})_4AgBiBr_8$ NB colloids (Fig. 2b). It was observed that the PL emission intensity was significantly enhanced at low temperatures compared to that at room temperature. The intrinsic pronounced quantum confinement effect in 2D layered perovskite make bound excitons easily formed.[12] The bound excitons could relax to self-trapped states and underwent radiative recombination, which is responsible for the broad PL emission (a shoulder at around 550 nm in Fig. 2b).[13] However, the bound excitons at self-trapped states were easily detrapped by thermal activation at higher temperatures (*i.e.*, at 300 K compared with 77 K), which caused the radiative transition down.[11] In contrast, at lower temperatures, as the thermal energy was reduced, the detrapping of bound excitons in self-trapped states by thermal activation was decreased, leading to enhanced radiative transitions

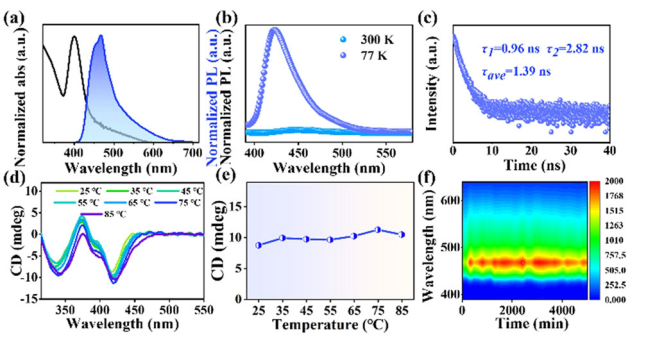

Fig. 2 (a) UV absorption and PL emission spectra of $(R\text{-MPEA})_4AgBiBr_8$ NBs. (b) Temperature-dependent PL spectra, (c) time-resolved PL decays spectra, (d) temperature-dependent CD spectra, (e) corresponding CD intensity at CD peaks of 420 nm and (f) PL intensity of $(R\text{-MPEA})_4AgBiBr_8$ NBs under ambient conditions with the relative humidity of RH = 65 ± 5%.

Published on 27 Diteli 2023. Downloaded on 19/07/2025 10:58:16 AM.

and increased PL emission intensity.[11,13] In addition, the photoluminescence quantum yield (PLQY) of (*R*-MPEA)$_4$AgBiBr$_8$ at room temperature was relatively low (0.06%) probably due to the competitive non-radiative transition by dimensional reduction from 3D to 2D, which was similar with findings in literature (about 0.01%, PEA$_4$AgBiBr$_8$).[14] The time-resolved photoluminescence (TRPL) decay spectrum of 2D (*R*-MPEA)$_4$AgBiBr$_8$ colloidal solution was measured (Fig. 2c). This result was fitted using a biexponential function and yielded an average PL lifetime of 1.39 ns, which is close to that of (*R*-MPA)$_4$AgBiI$_8$ (t_{ave} = 3.36 ns).[15] Differing from the previously reported achiral 3D $Cs_2AgInCl_6$, our 2D material possessed chirality through the introduction of chiral amine cation *R*-MPEA$^+$.[16,17] Differing from the chiral ammonium (Fig. S8, ESI†), Fig. 2d illustrated the presence of a distinct circular dichroism (CD) absorption located around their characteristic absorption peak (about 420 nm), which corresponded to the absorption edge. This bisignate CD pattern near the absorption edge with two peaks (*i.e.*, 370 nm and 420 nm) of chiral perovskite excitons can be attributed to the splitting of the energy state with the opposite spin state of electron perturbed by chirality, which is known as ''cotton effect''.[18] Notably, the CD peak at 335 nm can be ascribed to the additional CD response within the UV absorption band, due to transitions into the continuum (*i.e.*, above bandgap) states.[13] The g_{abs}-factor represents the magnitude of the CD signal, which indicates the difference in absorption of left-handed and right-handed circularly polarized light. The g_{abs}-factor of (*R*-MPEA)$_4$AgBiBr$_8$ NBs is determined to be -1.43×10^{-3} at 420 nm with optimized OAm amount (Fig. S9, ESI†). Even so, no detectable CPL peak was observed of these NBs solution, as depicted in Fig. S10 (ESI†). Besides, the temperature-dependent CD spectra of (*R*-MPEA)$_4$AgBiBr$_8$ NBs showcases a steady trend of CD signal (Fig. 2d and e), implying that these NBs remained undamaged and maintained good structural stability throughout the temperature range. The preservation of the chiral signal at elevated temperatures suggested that the chiral perovskite structure of the NBs was robust and resistant to thermal degradation, showing the potential for the application in optoelectronic devices. Similarly, it can be observed that the emission intensity of the colloidal solution showed just a small decline when it was subjected to the ambient environment for a prolonged period of 6000 minutes, as illustrated in Fig. 2f. Overall, these findings highlight the exceptional stability of the colloidal solution under normal atmospheric conditions and the structural resilience of the (*R*-MPEA)$_4$AgBiBr$_8$ NBs at elevated temperatures.

To confirm the significant influence of antisolvents on recrystallization, employment of common antisolvents such as chloroform and toluene were studied. Unfortunately, these single antisolvents did not endow the resultant product with desired chiroptical properties, even though distinct UV absorption or PL emission were observed (Fig. S11 and S12, ESI†). Also, the resulting morphology appeared in bulk shape or large particle precipitate without the characteristic nanoscale features (Fig. S13, ESI†).

By employing a chloroform/toluene mixture with a volume ratio of 2 : 3, narrower and irregularly shaped NBs were formed,

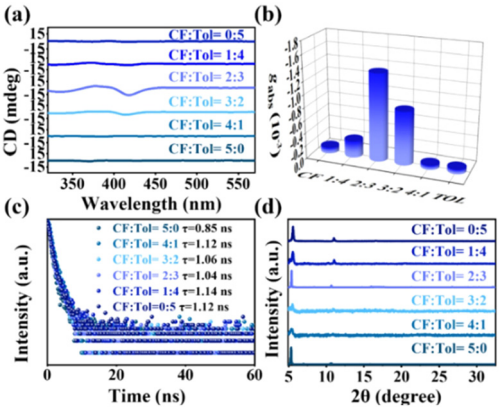

Fig. 3 (a) CD spectra, (b) g_{abs}-factor values at maximum CD peak, (c) TRPL spectra and (d) XRD patterns of 2D double (*R*-MPEA)$_4$AgBiBr$_8$ perovskites synthesized at different volume ratios of chloroform (CF)/toluene (Tol).

and these NBs exhibited a significant chiral optical signal, as evidenced by the CD spectra (Fig. 3a). The g_{abs}-factor reached its peak at -1.43×10^{-3}, as depicted in Fig. 3b. By introducing toluene and chloroform as antisolvents, it is possible to modulate the crystallization kinetics of the NBs. Toluene and chloroform, being solvents with different polarities, can have contrasting effects on the crystallization process. Therefore, by adjusting the ratio of toluene and chloroform in the antisolvent mixture, it is possible to control the rate and extent of crystallization, ultimately influencing the morphological features of the NBs. It has been established the chirality expression in perovskite is associated with particle size, with a decrease in the CD signal observed in larger particles.[19,20] Consequently, the differences in the morphological sizes of these double perovskite could be potential factors contributing to variations in CD responses. Furthermore, these double perovskites exhibited an average value of approximately 1 ns (Fig. 3c and Fig. S14, ESI†), indicating the volume ratio of antisolvents delivered little influence on the radiative process. Samples *via* different ratio mixtures with a relatively wider peak compared to the single antisolvent counterpart (Fig. 3d) revealed the presence of nanomaterials, which together with the Bi-based controls (Fig. S15, ESI†) suggested the successful synthesis of (*R*-MPEA)$_4$AgBiBr$_8$. The optimization of the solvent mixture composition allows for the enhancement of the chiral optical properties (Table S2, ESI†), providing valuable insights for tailoring the properties of chiral perovskite nanomaterials.

In order to achieve continuous tunability of excitonic emissions, the optical properties of the (*R*-MPEA)$_4$AgBiBr$_{8-8x}$I$_{8x}$ nanocrystals were investigated by introducing iodine into the reaction system, as depicted in Fig. S16a (ESI†). The solution emission colour transitioned from blue to green light by adjusting the iodine percentage. This transition was accompanied by a red-shift in both the UV absorption peak (from 405 nm to 505 nm) and the PL emission peak (from 450 nm to 570 nm) in Fig. S16b and c (ESI†). The red-shift can be ascribed to the change in energy band composition resulting from the substitution of bromine with iodine.[21] The XRD

 This journal is © The Royal Society of Chemistry 2023

Published on 27 Diteli 2023. Downloaded on 19/07/2025 10:58:16 AM.

patterns of the $(R\text{-MPEA})_4AgBiBr_{8-8x}I_{8x}$ (Fig. S16d, ESI†) revealed that the introduction of different ratios of iodine did not cause significant changes in the diffraction pattern, except for a slight shift of the diffraction peak towards smaller angles. This shift can be related to the larger size of the iodine anion. These findings are consistent with previous reports on the changes in crystal structure observed in 2D layered perovskite materials with different halide anion compositions.[9] The chiroptical activity of mixed halogen perovskite nanocrystals are shown in Fig. S16e and f (ESI†). While iodine or bromine perovskites exhibited significant CD responses, undetectable CD signals were obtained in the mixed halogen synthesized perovskites. This lack of CD signals in the mixed halogen perovskites suggested the presence of an uneven distribution of halide ions, indicating phase separation of bromine and iodine within the lattice framework.[22] This phase separation may hinder the formation of a chiral structure, resulting in the absence of chiral optical activity. Furthermore, the g_{abs}-factor of the iodine perovskite was measured to be -1.5×10^{-3}, which indicates that the iodine perovskite retains its chiral and optical activity, despite the absence of CD signals in the mixed halogen perovskites. These findings highlight the importance of understanding the influence of halogen composition on the chiral and optical properties of perovskite materials, and the need for precise control and uniform distribution of halide ions to achieve desired chiral and optical responses.

In conclusion, through the optimization of the antisolvent in the LARP process, we have successfully synthesized 2D lead-free chiral double perovskite $(R\text{-MPEA})_4AgBiBr_8$ with unique one-dimensional NB shape. These NBs exhibit significantly improved chiroptical signal, with a better symmetric CD response at around 420 nm and a g_{abs}-factor of approximately -1.43×10^{-3}, which is comparable to other 2D lead halide perovskite nanomaterials. By controlling the proportions of co-antisolvents, it is possible to optimize the morphology and chiral chiroptical response of these nanomaterials. It is found that the use of a co-antisolvent system is more effective than a single antisolvent in regulating the kinetics and chiral response of perovskite crystallization, enabling efficient expression of the chiral properties of the chiral ammonium molecules. This study opens up new research possibilities for investigating the influence of anti-solvent properties in ligand-assisted reprecipitation strategies on the chiral optical properties of nanomaterials. It also expands the scope of research on optoelectronic applications based on 2D lead-free nanomaterials.

The work was financially supported by the National Natural Science Foundation of China (No. 62104170 and 22109120), and the Zhejiang Provincial Natural Science Foundation of China (LQ21B030002 and LY23F040001).

Conflicts of interest

The authors declare no competing financial interest.

Notes and references

1 H. Y. Li, N. Shen, S. Chen, F. Guo and B. M. Xu, *Adv. Funct. Mater.*, 2023, **33**, 2214339.
2 T. B. Ji, T. Q. Niu and J. Wang, *et al.*, *J. Mater. Chem. A*, 2022, **10**, 13625.
3 Y. Y. Dang, X. L. Liu, B. Q. Cao and X. T. Tao, *Matter*, 2021, **4**, 794.
4 Z. Wen, R. Lu and F. Gu, *et al.*, *Adv. Funct. Mater.*, 2023, **33**, 2212095.
5 C. H. Chen, S. N. Cheng, L. Cheng, Z. K. Wang and L. S. Liao, *Adv. Energy Mater.*, 2023, **13**, 2204144.
6 T. Leijtens, R. Prasanna, A. Gold-Parker, M. F. Toney and M. D. McGehee, *ACS Energy Lett.*, 2017, **2**, 2159.
7 Y. Zhao, M. Dong and J. Feng, *et al.*, *Adv. Opt. Mater.*, 2022, **10**, 2102227.
8 J. B. Wu, S. H. You and P. P. Yu, *et al.*, *ACS Energy Lett.*, 2023, **8**, 2809.
9 R. Lu, Z. Wen and M. Zhao, *et al.*, *Adv. Opt. Mater.*, 2023, **11**, 2202290.
10 D. Li, X. Liu, W. Wu, Y. Peng, S. Zhao, L. Li, M. Hong and J. Luo, *Angew. Chem., Int. Ed.*, 2021, **60**, 8415.
11 X. Wang, K. Li, H. Xu, N. Ali, Y. Wang, Q. Shen and H. Wu, *Chem. Commun.*, 2020, **56**, 7917.
12 Y. Fang, L. Zhang, L. Wu, J. Yan, Y. Lin, K. Wang, W. L. Mao and B. Zou, *Angew. Chem., Int. Ed.*, 2019, **58**, 15249.
13 M. K. Jana, R. Song and H. Liu, *et al.*, *Nat. Commun.*, 2020, **11**, 4699.
14 M. Pantaler, V. Diez-Cabanes and V. I. Queloz, *et al.*, *JACS Au*, 2021, **2**, 136.
15 J. Wu, S. You and P. Yu, *et al.*, *ACS Energy Lett.*, 2023, **8**, 2809.
16 Y. Liu, A. Nag, L. Manna and Z. Xia, *Angew. Chem.*, 2021, **133**, 11696.
17 Y. Liu, M. S. Molokeev and Z. Xia, *Energy Mater. Adv.*, 2021, 2585274.
18 A. Ishii and T. Miyasaka, *Sci. Adv.*, 2020, **6**, eabd3274.
19 Y. Zhou, Z. Zhu and W. Huang, *et al.*, *Angew. Chem.*, 2011, **48**, 11658.
20 N. Tabassum, Z. N. Georgieva, G. H. Debnath and D. H. Waldeck, *Nanoscale*, 2023, **15**, 2143.
21 M. C. Weidman, M. Seitz, S. D. Stranks and W. A. Tisdale, *ACS Nano*, 2016, **10**, 7830.
22 L. Yan, M. K. Jana, P. C. Sercel, D. B. Mitzi and W. You, *J. Am. Chem. Soc.*, 2021, **143**, 18114.